Tech Memo
AERO 2211

UNLIMITED

Tech Memo
AERO 2211

ROYAL AEROSPACE ESTABLISHMENT

Technical Memorandum

March 1991

Asymmetric Vortex Flow Over Circular Cones

by

M. Pidd
J. H. B. Smith

Procurement Executive, Ministry of Defence
Farnborough, Hampshire

UNLIMITED

CONDITIONS OF RELEASE

0098384 301259

********** DRIC U

********** DRIC Y

Reports quoted are not necessarily available to members of the public or to commercial organisations

ROYAL AEROSPACE ESTABLISHMENT

Technical Memorandum Aero 2211

Received for printing 19 March 1991

ASYMMETRIC VORTEX FLOW OVER CIRCULAR CONES

by

M. Pidd

J. H. B. Smith

SUMMARY

Asymmetric vortex flow over circular cones is discussed in the light of predictions of the single-line-vortex model and of measurements made by Fiddes, Moir and Lean in the RAE 5m Wind Tunnel. For the case of separation lines specified as laterally symmetric, the space of conical solutions which contains the symmetric solutions of Bryson is explored thoroughly. No more than one pair of asymmetric solutions is found for each combination of a separation position and a ratio of incidence to cone semi-angle, except in a small region of the parameter space. The stability of the solutions to small asymmetric spatial disturbances is calculated. It emerges there is nowhere more than one stable solution, symmetric at smaller incidences, asymmetric at larger.

In contrast, the experiment, on a 10° semi-angle cone, with laminar separation, reveals many different levels of local side force, depending on roll angle, lengthwise station, and unit Reynolds number, as well as incidence. It is shown that the flow can be highly non-conical. At 35° incidence the flow may be developing streamwise towards a conical state, but this is not apparent at 30°. Analysis of the pressure distributions is complicated by an apparent turbulent re-attachment at the larger local Reynolds numbers.

This is a slightly extended version of the paper presented at the AGARD FDP Conference 'Vortex Flow Aerodynamics', Scheveningen, October, 1990.

LIST OF CONTENTS

1 INTRODUCTION

This Memorandum presents an update on earlier RAE work on the formation of asymmetric vortices from slender pointed bodies at large angles of incidence. The emphasis is on theoretical and experimental work on flow over circular cones.

The theoretical work began with the generalisation of Bryson's model[1] for symmetrical vortex flow over bodies of revolution to flows with lateral asymmetry. We formulated the model for asymmetric vortex flow over circular cones using slender-body theory, with arbitrarily chosen, straight separation lines, and the single line-vortex model of the separated flow. We looked for conical solutions, in which the line-vortices are straight, and eventually found a family of asymmetrical solutions[2]. When the separation lines are placed symmetrically on either side of the incidence plane, the symmetric solutions of Bryson occur, and the asymmetric solutions then bifurcate from this symmetric branch of solutions. The solutions depend only on the angular position of the separation lines and on the incidence parameter, defined as the ratio of the angle of incidence to the semi-angle of the cone. At values of the incidence parameter above that at which bifurcation occurs, a side force is predicted. This grows rapidly with the incidence parameter, reaching values comparable with the normal force, even though the separation lines are placed symmetrically. Quite large asymmetries in the positions of the separation lines, on the other hand, perturb the symmetric flow relatively little. This work pointed to an inviscid mechanism for the observed side force on slender pointed bodies.

This early work was followed by calculations using the more realistic vortex-sheet model, developed previously for symmetric flow on wings[3] and bodies[4]. This retains the framework of slender-body theory, separation is still specified along arbitrarily chosen straight lines, and the restriction to conical flow is retained. This work confirmed the conclusions reached previously about the primary role played by bifurcation and the limited importance of asymmetry in the positions of the separation lines. It also allowed favourable comparisons to be made with observations of vortex flow and with measured levels of side force[5,6]. The solutions are extended without difficulty to elliptic cones and it was demonstrated that a reduction in the vertical axis of the elliptic cross-section leads to an increase in the angle of incidence at which bifurcation from the symmetrical solution takes place[7]. Further work using this vortex-sheet method for more general shapes has been presented by Fiddes and Williams[8], and Williams[9].

The theoretical work in the present Memorandum is based on the simpler line-vortex model studied initially, so it is relevant at this point to discuss the relationship between the predictions of the two models. Fig 1 shows the starboard

side of a circular cone in symmetric flow at an incidence parameter of 3. A vortex sheet solution is shown, springing from the separation line S_S at the end of the horizontal diameter of the circular cross-section, and ending at E, with its core at C joined to E by the usual 'feeding sheet'. This separation position is typical for laminar separation. The arc identified by the figures 40^o-49^o is the locus of the vortex positions in the line-vortex model for angular positions of the separation line, S_V, of between 40^o and 49^o above OS_S. The first point to be made is that this locus passes very close to C, indicating that the predictions of the simple model have a certain resemblance to those of the better model. The second point is that this resemblance is found for positions of the separation line in the simpler model which lie well to leeward of the position in the better model. The reason for this is brought out by the difference in the shape of the separating stream surface. For the better model this is the vortex sheet S_SBE. For the simpler model, the separating stream surface springs from the separation line S_V, which is a typical conical-flow stagnation point, so that it takes a course similar to that indicated by the arrow. Because the initial part of the vortex sheet, S_SB, lies relatively close to the surface of the cone, similar flows near C are generated with very different separation positions in the two models. The position of point B has been chosen so that the circulation in the sheet model about the core C and the segment BE is the same as the circulation in the line-vortex model with separation at S_V.

Before leaving this discussion of the theoretical models it is appropriate to mention the prediction of asymmetric vortex flow by more complete models. For inviscid supersonic flow over cones, conical solutions of the Euler equations governing the flow exist. Such solutions displaying lateral asymmetry have been obtained by Marconi[10], who forced the occurrence of primary separation along symmetrically located separation lines. Agreement between these solutions and those of the vortex-sheet model in slender-body theory was pointed out by Fiddes and Williams[8]. For laminar viscous flow, as described by the Navier-Stokes equations, conical flows do not exist. However, a slightly modified equation set does display conical solutions for supersonic speeds. Asymmetric solutions of these equations for flows past circular cones have been obtained by Siclari and Marconi[11]. These display slight asymmetry in the position of the primary separation lines. Secondary separation also occurs, but in their overall features the flows are not markedly different from the Euler solutions of Marconi[10] and the vortex-sheet solutions of Fiddes[4].

On the experimental side, it is quite impossible to review the investigations which have been carried out within the space of this introduction. A comprehensive review was provided by Hunt[12] in 1982. Since we are particularly interested in the flow over circular cones, we shall make extensive use of the measurements made by Fiddes, Lean and Moir[13] in the 5 metre Tunnel at RAE and briefly reported in Ref 14. Details of their wind-tunnel model are shown in Fig 2. The model is large, enabling quite detailed measurements to be made on the conical portion, which extends 700 mm from the apex, and the tunnel is pressurised, enabling Reynolds number to be varied at constant Mach number. The model mounting allows the roll angle to be set from outside the tunnel. Since we are interested in the flow over cones, we shall consider the results of pressure measurements made at the first four measuring stations, all of which lie on the conical portion of the model. Note that the semi-angle of the cone is 10°, so that the incidence parameter takes the values 3.0 and 3.5 at the angles of incidence 30° and 35° which we shall consider. Conical vortex-sheet solutions exist for these values for a range of separation line positions near those occurring experimentally, for both symmetric and asymmetric flows. The pressure holes are spaced at 10° intervals circumferentially round the body at all measuring stations, which are themselves equally spaced. The interval in the circumferential direction limits the accuracy with which the local side-force coefficient can be determined.

Fig 3 shows an example of the results obtained. The local side-force coefficient, C_Y, based on the local diameter of the cone, is plotted against the angle of roll, ϕ, about the axis of the cone. The angle of incidence, α, is 35°, the results are for the first station, and the tunnel pressure is only just above atmospheric, so that the boundary layer growing from the windward generator is laminar at the separation line. We see that, at about half of the selected values of roll angle, the side force takes an approximately uniform numerical value, approaching in magnitude the local normal-force coefficient, C_N, shown on the upper curve. As usual, the sign of C_Y changes several times in a complete revolution about the axis. At about half the remaining values of ϕ, C_Y is small enough for us to believe that the flow is essentially symmetric. All this is consistent with the predictions of the inviscid model, that symmetric solutions and asymmetric solutions of right- and left-handed forms both occur. However, the remaining quarter of the points show values of side force which are clearly intermediate between zero and the extreme value. These correspond to neither the symmetric nor the asymmetric solutions. It is these intermediate values which provoked the work to be described below.

The theoretical component of this work started with a complete exploration of the parameter space of the existing symmetric and asymmetric solutions of the line-vortex model for conical flow, with the intention of finding further solutions which might yield intermediate levels of side force. No further bifurcation locus was found, however, and the small regions of the parameter space in which multiple solutions do occur turn out to be insignificant. This work is described in section 2. A formulation of the same model for non-conical flow made it possible to examine the stability of the conical solutions to small non-conical spatial disturbances. This examination shows that the significant asymmetric solutions are stable, but the symmetric solutions are only stable at values of the incidence parameter below that at which asymmetric solutions occur. In fact, bifurcation takes place 'with exchange of stabilities', see for instance, Ref 15. The stability study is described in section 3.

This leaves the explanation of Fig 3 in a worse state than before. No only are we reasonably sure that no further solutions exist, but the co-existence of symmetric and asymmetric solutions for the same incidence parameter and separation position is unlikely. The possibility of unsteadiness in the flow was considered, the idea being that the pressure instrumentation would record an average value if the flow state alternated between its right- and left-handed asymmetric forms, spending a proportion of the total time in each which depended on roll angle. If this occurred, the pressure distribution at a particular roll angle could be constructed from an appropriate linear combination of the pressure distributions at roll angles which correspond to the right- and left-handed asymmetric forms. Many, though not all, of the measured pressure distributions could be constructed in this way, as shown in unpublished work by D.E. Lean. Consequently, Earnshaw and Rae undertook a brief, and also unpublished, investigation in which an unsteady pressure transducer was mounted in the model and its output monitored visually at a range of roll angles. The frequency response of the system was sufficient to resolve events on a time scale corresponding to the passage of a fluid particle from the apex to the measuring station. No significant variation in amplitude of the observed fluctuations was detected between roll angles at which the side force took extreme and intermediate values. This explanation of the intermediate levels of side force was therefore abandoned.

It was only at this stage that we considered the possibility that the flows giving rise to the local side-force distributions in Fig 3 might not be even approximately conical. Evidence for the non-conicality of some of the flows at $\alpha = 35^{o}$ is presented in section 4. This leads to a tentative explanation for the occurrence of intermediate and near-zero levels of side force, supported by

further features of the stability theory. The outcome is not entirely conclusive, partly because data were only taken at the first two measuring stations for $\alpha = 35^{\circ}$.

This less than conclusive outcome led us to examine the results at $\alpha = 30^{\circ}$, for which data at all six stations are available. At this lower angle of incidence, the side force levels are lower, though still significant, and the intermediate states occur as the rule rather than the exception. Significant effects of Reynolds number also appear, but the results indicate that the underlying vortex flow structure is markedly non-conical for most of the range of roll angles. Details are given in section 5.

Finally, in section 6, an attempt is made to summarize our present understanding of steady vortex flow over circular cones.

2 SOLUTIONS OF THE LINE-VORTEX MODEL FOR CONICAL FLOW OVER CIRCULAR CONES

In an attempt to explain the occurrence of the intermediate levels of side force shown in Fig 3, the solution space of the line-vortex model of Ref 2 was explored more thoroughly. The essential features of the model are illustrated in Fig 4. A pair of line-vortices OV_1 and OV_2 lie downstream of the pointed apex O of the body. Their circulations are Γ_1 and $-\Gamma_2$. Each is joined by a feeding vortex-sheet to a separation line OS_1 or OS_2 on the surface of the body. These feeding sheets are surfaces of discontinuity in the velocity potential, with the magnitude of the jump depending only on the streamwise variable x , that is to say, as vortex-sheets in which the vortex-lines are transverse to the main stream. The velocity field is constructed using slender-body theory and two conditions are formulated. We require in the first place that each vortex system, comprising a line-vortex and its feeding sheet, is free of transverse forces. This is achieved by balancing the force arising from the pressure difference across the feeding sheet by a force acting on the line-vortex. The second condition expresses the occurrence of separation. It forces the velocity vector at the separation line OS to lie along OS . Both these conditions are gross simplifications of the conditions that a vortex-sheet model would satisfy, but they provide a representation of the principal kinematic and kinetic constraints on the vortex flow.

Fig 4 is drawn for conical flow over a circular cone, but it is straightforward to write the conditions for non-conical flow and a general body of revolution. With the axes as shown, we introduce the complex variable

$$Z = y + iz$$

in the cross-flow plane, and define the vortex positions by

$$Z = Z_1(x) \quad \text{and} \quad Z = Z_2(x) \ .$$

Then, the condition of zero transverse force on the starboard vortex system can be expressed as

$$(\bar{Z}_1 - ae^{-i\theta_1})U\frac{d\Gamma_1}{dx} + U\Gamma_1\frac{d\bar{Z}_1}{dx} +$$

$$\Gamma_1\left[i\alpha U\left(1 + \frac{a^2}{Z_1^2}\right) - \frac{aU}{Z_1}\frac{da}{dx} + \frac{\Gamma_1\bar{Z}_1}{2\pi i\left(Z_1\bar{Z}_1 - a^2\right)} + \frac{\Gamma_2}{2\pi i}\left(\frac{1}{Z_1 - Z_2} - \frac{\bar{Z}_2}{Z_1\bar{Z}_2 - a^2}\right)\right] = 0 \ . \qquad \ldots\ldots(1)$$

Here Γ_1 and $-\Gamma_2$ are the circulations of the vortices, a is the local radius of the body, and the separation line, OS_1, lies along $Z = ae^{i\theta_1}$. The first term represents the force on the feeding sheet, the second term represents the force on the line-vortex due to its inclination to the free stream, and the third term represents the force on the line-vortex due to the cross flow. Equation (1) represents a straightforward generalisation of the corresponding equations in Ref 1, dealing with laterally-symmetric flow, and in Ref 2, dealing with asymmetric but conical flow. The corresponding equation for the port vortex system has the suffixes 1 and 2 interchanged. The generalised Kutta condition representing the occurrence of separation on the starboard separation line is

$$\frac{\Gamma_1(Z_1\bar{Z}_1 - a^2)}{2\pi|Z_1 - ae^{i\theta_1}|^2} - \frac{\Gamma_2(Z_2\bar{Z}_2 - a^2)}{2\pi|Z_2 - ae^{i\theta_1}|^2} = 2a\alpha U\cos\theta_1 \ , \qquad (2)$$

provided the angular position, θ_1, of the separation line is independent of x. The corresponding equation for the port side is obtained on replacing θ_1 by θ_2.

For a slender circular cone of semi-angle δ, we have

$$a = \delta x \ , \qquad (3)$$

and we can introduce non-dimensional variables ζ and γ by

$$Z_j = a\zeta_j \ , \quad \Gamma_j = 2\pi a\delta U\gamma_j \ , \quad j = 1,2 \ . \qquad (4)$$

Then (2), and the corresponding equation for the port side, become

$$\frac{\gamma_1(\zeta_1\bar{\zeta}_1 - 1)}{|\zeta_1 - e^{i\theta_1}|^2} - \frac{\gamma_2(\zeta_2\bar{\zeta}_2 - 1)}{|\zeta_2 - e^{i\theta_1}|^2} = 2\frac{\alpha}{\delta}\cos\theta_1$$

$$\frac{\gamma_1(\zeta_1\bar{\zeta}_1 - 1)}{|\zeta_1 - e^{i\theta_2}|^2} - \frac{\gamma_2(\zeta_2\bar{\zeta}_2 - 1)}{|\zeta_2 - e^{i\theta_2}|^2} = 2\frac{\alpha}{\delta}\cos\theta_2 \quad . \tag{5}$$

Introducing a non-dimensional streamwise variable ξ by

$$x = x_0 e^{\xi} \quad , \tag{6}$$

where $x_0 > 0$ is a constant to be interpreted in section 3, we find (1) becomes

$$\frac{d}{d\xi}\left[\gamma_1(\bar{\zeta}_1 - e^{-i\theta_1})\right] = \gamma_1 F(\zeta_1,\zeta_2,\gamma_1,\gamma_2,\theta_1,\alpha/\delta) \quad , \tag{7}$$

where $F(\zeta_1,\zeta_2,\gamma_1,\gamma_2,\theta_1,\alpha/\delta) =$

$$e^{-i\theta_1} - 2\bar{\zeta}_1 - i\frac{\alpha}{\delta}\frac{\zeta_1^2 + 1}{\zeta_1} + \frac{1}{\zeta_1} + \frac{i\gamma_1\bar{\zeta}_1}{\zeta_1\bar{\zeta}_1 - 1} + \frac{i\gamma_2(\zeta_2\bar{\zeta}_2 - 1)}{(\zeta_1 - \zeta_2)(\zeta_1\bar{\zeta}_2 - 1} \quad . \tag{8}$$

The corresponding equation for the port side becomes

$$\frac{d}{d\xi}\left[\gamma_2(\bar{\zeta}_2 - e^{-i\theta_2})\right] = \gamma_2 F(\zeta_2,\zeta_1,\gamma_2,\gamma_1,\theta_2,\alpha/\delta) \quad . \tag{9}$$

For conical flow, the non-dimensional variables ζ_j, γ_j and θ_j that describe the vortex systems are independent of the streamwise coordinate, so the governing equations reduce to

$$F(\zeta_1,\zeta_2,\gamma_1,\gamma_2,\theta_1,\alpha/\delta) = F(\zeta_2,\zeta_1,\gamma_2,\gamma_1,\theta_2,\alpha/\delta) = 0 \tag{10}$$

and the generalised Kutta conditions (5). Equation (10) consists of two complex equations, equivalent to four real equations, so that we have six equations in

all to determine the two coordinates of each vortex and their circulations. The parameters on which the solutions depend are the incidence parameter α/δ and the positions θ_1 and θ_2 of the separation lines.

Some solutions given in Ref 2 for symmetrically placed separation lines illustrate the generation of asymmetric solutions by bifurcation from the symmetric branch as the incidence parameter increases above a critical bifurcation value. This framework is extended in Ref 5, dealing with vortex-sheet solutions, to embrace solutions with asymmetric separation lines. The symmetric solutions are extended to a first family of solutions, comprising those solutions which either are symmetric or become symmetric when asymmetry in the separation line position is gradually reduced to zero, with α/δ held constant. The asymmetric solutions are extended to a second family of solutions in which the asymmetry in the solution persists when the asymmetry in the positions of the separation lines is reduced to zero. The level of side force is shown to depend primarily on the family to which the solution belongs and to a lesser extent on any asymmetry in the separation line position. Chin and Lan[16] reach a similar conclusion for their line-vortex model. Little asymmetry in separation line position is observed experimentally by Rainbird *et al*[17] for turbulent separation and by Mundell[18] for laminar separation and little is calculated for laminar flow at asymptotically large Reynolds number by Fiddes and Smith[7], so we believe that the loss of generality involved in restricting our attention to symmetrically-placed separation lines is acceptable.

We therefore set

$$\theta_1 = \theta \quad \text{and} \quad \theta_2 = \pi - \theta \tag{11}$$

and consider the dependence of the solutions on the two parameters α/δ and θ only. We note in passing that, when we seek a symmetrical solution with $\gamma_2 = \gamma_1$ and $\zeta_2 = -\bar{\zeta}_1$, in addition to (11), equations (5) become identical, while by (8)

$$F(\zeta_2,\zeta_1,\gamma_2,\gamma_1,\theta_2,\alpha/\delta) = -\bar{F}(\zeta_1,\zeta_2,\gamma_1,\gamma_2,\theta_1,\alpha/\delta) \quad .$$

Hence the four equations (7) and (9) reduce to two, leaving three real equations for the three unknowns. For this simple, symmetrical problem, Moore[19] showed how the governing equations could be reduced to a single algebraic equation of the 17th degree and in this way all possible solutions could be found. We have preferred to use a multivariable generalisation of Newton's iterative method to solve the nonlinear equations, since Moore's reduction cannot be carried through

for the asymmetric problem. This is based on the simple idea that if $\underline{x} = \underline{x}_0$ is a close enough approximation to a solution of the set of equations

$$\underline{F}(\underline{x}) = 0$$

then

$$\underline{x} = \underline{x}_0 - J^{-1}(\underline{x}_0)\underline{F}(\underline{x}_0) \tag{12}$$

is an even closer approximation, where $J(\underline{x})$ is the Jacobian matrix of the functions $\underline{F}(\underline{x})$ with respect to the arguments $\underline{x}$. This method is well suited to exploring a connected space of solutions, since each solution is accessible from a neighbouring solution which is a close approximation to it. In fact, as Moore found, all the solutions to the symmetric problem do form a connected surface lying in a multidimensional space, so they could all be found by the present Newton method. The range of solutions is illustrated in Fig 5. The Figure represents the projection of the solution surface onto the plane of the solution parameters θ and α/δ. The curve ABD is the projection of the edge of the surface along which the vortices reach the surface of the cone and their strength vanishes. The curve is given by

$$\frac{\alpha}{\delta} = \frac{3}{2}\,\mathrm{cosec}\,\theta$$

which is often referred to as the lower bound for solutions. In fact it is only the lower bound to the right of point B, which lies at $\theta = \theta_c \approx 46.1^\circ$,

where $\tan\theta_c = \frac{3\sqrt{3}}{13}$ and $\frac{\alpha}{\delta} = \sqrt{\frac{13}{3}} \approx 2.08$.

To the left of point B there are solutions for values of α/δ less than 1.5 cosec θ, lying in the region between the curve BD and the curve BC. The curve BC is simply the edge of the projection of the solution surface. The corresponding curve on the solution surface is not special: in particular, there are neighbouring points of the solution surface on both sides of it. Consequently the projection of the surface is folded along BC and we can call BC a fold-line of the projection. Two points of the solution surface are projected onto every point of the $(\theta,\alpha/\delta)$ plane between the curves BD and BC, so that two solutions exist for each pair of values of θ and α/δ in this region. The significance of the remaining curve AEB appears when we consider the symmetric solutions as one branch of the set of solutions of the equations (5) and (10) with (11), which govern the flow when symmetry is not assumed. The solution surface now lies in a space of even more dimensions, and it now contains

a double curve, or curve of double points, along which bifurcation takes place, so that two branches of the surface intersect along the double curve. The projection of this curve onto the $(\theta,\alpha/\delta)$ plane is the bifurcation locus shown as AEB in Fig 5. It can be shown that the determinant of the Jacobian matrix used in the solution process vanishes on the bifurcation locus, so the locus can be identified by monitoring the sign of this determinant as the symmetric branch of the solution is explored. The vanishing of $|J|$ on the bifurcation locus makes the use of the Newton method difficult near it, and various schemes to avoid this difficulty have been used. It can also be seen that $|J|$ vanishes on the fold line, but the solution surface can be explored near there by stepping in one of the vortex coordinates instead of θ or α/δ .

We now turn to the corresponding picture for the asymmetric solutions, Fig 6. The curve AEB is the bifurcation locus, the same curve as in the previous Figure. Asymmetric solutions arise when α/δ is increased, at constant θ , from points on the bifurcation locus. Once again, there are edges to the surface of solutions where one of the vortices reaches the surface of the cone. The projections of these edges are the curves BJG and AHA . Also, once again, there is a fold line FG which results from our choosing to project onto the $(\theta,\alpha/\delta)$ space, rather than any intrinsic feature of the solution itself. There is now an extra boundary of the region of consistent solutions. This is not a feature of the system of equations, but arises from the simplifications made in constructing the model. The condition applied at separation, that the velocity is parallel to the separation line, is also satisfied at an attachment line, so that further consideration is necessary[2], as indicated in the inset in Fig 4, to distinguish between the two possibilities. In the region labelled 'inconsistent' in Fig 6 one of the postulated separation lines is, in fact, an attachment line.

The small region of intersecting curves in Fig 6 is enlarged in Fig 7. Two curves from Fig 5 have been added, so that the Figure now indicates the regions of existence of both symmetric and asymmetric solutions in this small part of the $(\theta,\alpha/\delta)$ plane. Following up the account of the asymmetric solutions, we see them occurring above the bifurcation locus BFJE . It is easiest to trace the solution surface by moving downwards and to the left from the edge BJ of the surface where the vortex lies on the cone. Then we find either that the asymmetric solutions disappear when the lower part BF of the bifurcation locus is encountered, or the solution surface folds back on itself at the fold line FG . The asymmetric solutions then extend upwards and to the right in the region bounded below by the portion FJE of the bifurcation locus. Note that there is a narrow region between the fold line FG , the edge JG' and the portion FJ of the

bifurcation locus in which there are two pairs of asymmetric solutions for each choice of θ and α/δ .

Our search for additional solutions has therefore led us into this narrow region of the parameter space. When the side forces corresponding to the different pairs of asymmetric solutions in this region are calculated, they turn out to be quite similar, so they do not correspond to the flows with the very different levels of side force that are illustrated in Fig 3. Monitoring the signs of $|J|$ over the solution surface revealed no further changes of sign, so we conclude that no further bifurcation occurs at values of α/δ up to 10. There might be other solutions which are not connected to the solution surface we have explored, but there is no simple way to search for them.

It seems unlikely that more elaborate models of the flow, based on vortex sheets, the Euler equations, or the Navier-Stokes equations, would display more significant regions of multiple solutions of a conical or quasi-conical nature.

3 STABILITY OF CONICAL FLOWS

The situation depicted in Figs 5 to 7 is of a confusing variety of solutions of the model for conical flows over circular cones. We now put forward a stability argument which indicates which of these solutions is likely to correspond to the flows that actually occur.

The disturbances which we treat in the stability analysis are spatial rather than temporal. We suppose that a conical flow solution occurs and then, at some lengthwise station, $x = x_0$, a small disturbance is introduced into the flow, taking the form of small changes in the positions and strengths of the vortices. Since we are using slender-body theory, no upstream effect of the disturbance is possible. We investigate the initial rate of change of this disturbance in the downstream direction. If all disturbances decay, we say that the solution is stable, while if any disturbance grows, we say that the solution is unstable.

The disturbed flow is clearly non-conical, but the body shape is still a circular cone. For simplicity we assume that the separation lines are not altered by the disturbance, and that the vortex strengths are still coupled to the positions through the generalised Kutta conditions. (Some calculations with the vortex strengths unaffected by the disturbances to their positions showed stability boundaries very slightly displaced.) Then the governing equations (5) to (9), together with (11) for the particular solutions with symmetric separation are considered.

For convenience, we introduce new variables v_1, v_2, v_3, v_4 by

$$\begin{aligned} v_1 + iv_2 &= \gamma_1\left(\bar{\zeta}_1 - e^{-i\theta_1}\right) \\ v_3 + iv_4 &= \gamma_2\left(\bar{\zeta}_2 - e^{-i\theta_2}\right) \quad . \end{aligned} \tag{13}$$

Since we are concerned with small disturbances about a conical solution we write each variable as the sum of a term independent of ξ, with suffix c, and a small quantity, identified by a prime, thus:

$$\zeta_j(\xi) = \zeta_{jc} + \zeta_j'(\xi) \ , \quad \gamma_j(\xi) = \gamma_{jc} + \gamma_j'(\xi) \ , \qquad j=1,2;$$

$$v_j(\xi) = v_{jc} + v_j'(\xi) \ , \qquad j = 1,2,3,4. \tag{14}$$

When these are introduced into (5) and (13), and products of small quantities are neglected, the resulting equations are linear and homogeneous in the small quantities, so that ζ_1', ζ_2', γ_1' and γ_2' can be expressed in terms of v_1', v_2', v_3' and v_4' with constant coefficients depending on the conical solution quantities with suffix c. With ζ_1', ζ_2', γ_1' and γ_2' expressed in this way, the introduction of (14) into (7) and (9) leads to four real equations which can be written in matrix form as

$$\left\{\frac{dv_i'}{d\xi}\right\} = J_1\left\{v_j'\right\} \ , \tag{15}$$

where the matrix J_1 is the Jacobian matrix of the real and imaginary parts of the right-hand sides of (7) and (9) with respect to the variables v_i. Its elements depend on the conical solution, but not on ξ. J_1 is almost, but not quite, the same as the matrix J used to solve the conical flow problem by Newton's method (12). In fact

$$J_1 = \begin{bmatrix} \gamma_1 & 0 & 0 & 0 \\ 0 & \gamma_1 & 0 & 0 \\ 0 & 0 & \gamma_2 & 0 \\ 0 & 0 & 0 & \gamma_2 \end{bmatrix} J \quad . \tag{16}$$

Now (15) is a system of four first-order linear differential equations with constant coefficients. The standard treatment (theorem 8.11 of Ref 20 for example) shows that the stability of the system depends only on the real parts of

the eigenvalues of J_1 . We have stability if the real parts are all negative and instability if any eigenvalue has a positive real part. The complications arising for eigenvalues with zero real part can be ignored for present purposes. The consequence of instability is that a disturbance with a component in the direction of the eigenvector of the appropriate eigenvalue will grow exponentially in ξ , as long as it remains small enough for the linearised treatment to apply. In particular, if the largest real part is $\lambda_r > 0$, the growth is like

$$e^{\lambda_r \xi} = \left(\frac{x}{x_0}\right)^{\lambda_r} ,$$

by (6). The growth rate in x is therefore algebraic rather than exponential, and it is the more rapid the nearer to the apex the disturbance is introduced.

The solution surface described in the previous section, both symmetric and asymmetric branches, was re-explored, evaluating the eigenvalues of J_1 along the way. From this evaluation and the preceding discussion the stability or instability of the solutions can be identified. For the symmetric branch the outcome is shown in Fig 5. We recall that the disturbances under consideration are not restricted to being symmetric. The only symmetric solutions stable to general disturbances are in the region ABEA, the multiple solutions are unstable. The change in stability takes place across the bifurcation locus, since the matrices J and J_1 are related by (16).

For the asymmetric branch, Fig 6 shows the asymmetric solutions are generally stable. Exceptions arise in the region BFGJB, part of which is shown on a larger scale in Fig 7. The asymmetric solution branch which arises from bifurcation along the arc BF and extends as far as the edge BJG' comprises unstable solutions only. On the other hand, the asymmetric solution branch which arises from bifurcation along the arc FJE comprises stable solutions. Consequently, in the region FGG'J there are two branches of asymmetric solutions, one stable and one unstable, in addition to the symmetric branch, which is unstable. Stable solutions only occur above and to the right of the hatched boundary and nowhere is there more than a single stable symmetric solution or a pair of asymmetric solutions. Hence the consideration of the stability is enough to resolve the multiplicity of solutions. This supports the view that the occurrence of asymmetry in the real flow is due to hydrodynamic instability rather than, say, to differential transition in the boundary layers on the two sides of the cone.

Larger values of α/δ are unrealistic, because the theory assumes α is a small angle and very small values of δ are of no practical significance. The figures show therefore that a value of θ larger than 30° is required to produce a realistic, stable solution. This is less restrictive than appears initially, in view of the earlier conclusion, based on Fig 1, that the separation line position in this model is well to leeward of the separation line in a more representative model.

Although the distinction between stable and unstable solutions is of theoretical importance, in a practical situation the growth rate of disturbances also plays an important part. Here we are concerned with spatial disturbances and there is only a finite length of body over which they can grow. It is therefore interesting to see the actual values of the largest real part, λ_r, of the eigenvalues of the matrix J_1. For symmetric separation lines 56° beyond the mid-plane of the body, these quantities are displayed as functions of the incidence parameter in Figs 8 and 9. At small values of α/δ there is no solution. Just above 1.8, a symmetric solution becomes possible. This is initially stable and the eigenvalue is negative, though numerically very small, so that disturbances would decay very slowly, and conversely evolution towards it from a neighbouring non-conical solution would be very slow. At a value of α/δ of about 2.08, bifurcation occurs and the eigenvalue of the symmetric solution becomes positive. The eigenvalue of the asymmetric solution is negative corresponding to its stability. The eigenvalues grow numerically, but remain small for $\alpha/\delta \leqslant 5$. The kink in the curve for the asymmetric solution at $\alpha/\delta \approx 3.8$ corresponds to the eigenvalue becoming complex at the larger values.

The small values of λ_r suggest that, if we are prepared to admit solutions that are not exactly conical, then approximately symmetrical and highly asymmetrical solutions may be found for the same value of α/δ, despite the outcome of the stability analysis for the conical solutions.

4 MEASUREMENTS ON A 10° CONE AT $\alpha = 35^{\circ}$

The experiment, using the model shown in Fig 2, was designed so as to ensure that the flow was as nearly conical as possible at the first ring of pressure holes, at the lowest total pressure available (110 kPa). The shape of the model is conical for several local diameters downstream of this station and the Reynolds number is low enough for the boundary layer to be laminar at the primary separation line. The direct evidence for the state of the boundary layer is the visualisation based on the difference in evaporation rate of methylsalicicylate held in a film of china-clay, carried out by Moir[21]. Fig 10 is reproduced from

his paper. Note that his observation is for $\alpha = 30^{\circ}$, at a Mach number of 0.2 and a total pressure of 2 atmospheres. The present results are for $\alpha = 35^{\circ}$, at a Mach number of 0.15 and a total pressure of 1.1 atmospheres. We may suppose that the tunnel temperatures are the same. We cannot allow for the difference in angle of incidence, but differences in total pressure and Mach number simply lead to the prediction of a different streamwise location at which transition begins to affect the separation line. Note also that the streamwise location at which the separation line first encounters a turbulent wedge depends on where the wedge originates along the transition front. Even with the wedge on the separation line, this still leaves separation laminar all along the conical part of the model for the test conditions of Fig 3.

However, when the local side force coefficients at the first two stations are compared, it becomes clear that the flow at many roll angles is not conical. Fig 11 illustrates this. The peak levels of C_Y at the two stations are slightly different, so the values at each station have been normalised with respect to the peak value of $|C_Y|$ at that station. The resulting values at the two stations are then plotted and the values at station 1 are joined to those at station 2 by arrows, so the arrow indicates the direction of the flow development. There are several short arrows close to the extreme states and two short arrows near the zero axis: these may well correspond to conical flow conditions. There are also several longer arrows, which reach, or approach, the extreme values: these seem to correspond to flows which are evolving towards the extreme states. Certainly, the extreme values are more common at station 2. Finally, there are several arrows which lie away from the extreme values and often also point away from the extreme values. If these are evolving toward the extreme states, it is clear that they have a long way to go. Many of these arrows are long, indicating a marked non-conicality. It is clear that all the intermediate side-force levels at station 1 have long arrows leading from them, so they must correspond to non-conical states. Many of these flows have reached, or are approaching, extreme states, which are probably conical, by station 2. Unfortunately, measurements further downstream at this angle of incidence are not available, so their further evolution cannot be traced. Pressures were measured at all stations at $\alpha = 30^{\circ}$ and these results are considered in section 5.

The appearance of conical flows with extreme or zero values only is consistent with the solutions of the simple flow model and the predominance of extreme values is consistent with the stability analysis. To obtain a more complete explanation, we need to consider what happens close to the apex of the tunnel model. We note first that, since the model imperfections are finite, their

size relative to the local diameter increases without limit as the notional apex is approached. Secondly, we note that such understanding of the flow as we have is based on concepts relevant at high Reynolds numbers, while the local Reynolds number tends to zero as the apex is approached. Our flow model can therefore only apply downstream of some station whose distance from the notional apex depends on the scale of the imperfections due to manufacture and handling of the tunnel model and on the unit Reynolds number* of the test. At this station we must suppose that the initial conditions for the system of ordinary differential equations (7) and (9) may be quite unrelated to the symmetric or asymmetric solutions with which we are familiar. We should, therefore, not be surprised if non-conical flows are sometimes observed. It is the preponderance of approximately conical flows that requires explanation. The outcome of the stability analysis, that disturbances to stable conical solutions decay like $(x/x_0)^{\lambda_r}$ and disturbances to unstable conical solutions grow in the same way, with $\lambda = \lambda_r$ illustrated in Figs 8 and 9, does show that the evolution either towards or away from conical solutions may be slow, even when the flow is close to being conical.

It is natural to ask what additional light the actual pressure distributions throw on this discussion. Let us start, for simplicity, with $\phi = 330^\circ$, at which the side force is nearly zero at both stations, as seen in Fig 11. The pressure levels are slightly different at the two stations, so the pressure coefficients have been adjusted to agree on the windward generator in preparing Fig 12. Here the crosses represent C_Y at station 1, and the circles the adjusted values at station 2. We see, with some relief, that both the distributions are almost symmetrical, but they are clearly very different. The interpretation must be doubtful in the absence of further evidence; however it appears that laminar separation is occurring at much the same angular positions, indicated by the arrows, at each station, and that some degree of turbulent reattachment occurs at station 2, allowing a further rise in surface pressure to occur. Fig 13 is the comparable plot for $\phi = 180^\circ$, for which the two stations again give almost the same side force, but now at a maximum value. We again see a laminar separation on both sides at station 1 and probably laminar separation with a degree of turbulent reattachment at station 2. However, the initial separation on the left of the Figure seems some 20° further to leeward at station 2. We now turn to a roll angle, Fig 14, for which Fig 11 shows a substantial reduction in side force between stations 1 and 2. The pressure distribution at station 1 (crosses) now shows two well-marked suction peaks under separation vortices. This

* Reynolds number per unit length, U/ν, a dimensional quantity.

suggests that the flow structure is quite different from that in the extreme state shown in Fig 13, for which only one pronounced suction peak arises, under the vortex that is nearer to the surface. At station 2, the separation seems to take place further to leeward on both sides. The reduction in side force does not seem to be associated with any approach to symmetry in the pressure distribution.

In view of the decision to confine attention to separation lines which are symmetrically placed, it is appropriate to present the limited evidence for the location of separation provided by the measured pressure distributions. On the assumption that separation is followed by a pressure plateau, we can estimate the position of separation to 5° in azimuthal angle, *ie* half the spacing of the pressure holes. For station 1 at $\alpha = 35^\circ$ the pressure distributions at 21 values of the roll angle were examined in this way. It emerges that the mean of the separation angles on the two sides is 102.5°, to within 2.5°, and the displacement of each line from this mean correlates with side-force coefficient, rising to a maximum of 10° for the extreme values of side force.

5 MEASUREMENTS ON A 10° CONE AT $\alpha = 30^\circ$

At smaller angles of incidence, the variation of side force with roll angle is not dominated by the occurrence of extreme states. Fig 15 shows the variation of the local side-force coefficient at station 1 for $\alpha = 30^\circ$ and the same Mach and Reynolds numbers as Fig 3. The local normal-force coefficient is also shown for comparison. At this lower incidence, the side force is smaller, absolutely and in relation to the normal force, but it is still significant. There is no obvious correlation between the side and normal force.

At this angle of incidence we have local side-force values at all six measuring stations, of which the first four lie on the conical part of the model, as shown in Fig 2. We shall use values at these four stations to assess the degree of conicality of the flow. We also have values measured at three different levels of total pressure in the wind tunnel, 110 kPa, 200 kPa and 300 kPa, providing three unit Reynolds numbers at the same Mach number, $M = 0.15$.

Fig 16 shows the variation of the local side-force coefficient with roll angle at the first three measuring stations at atmospheric pressure. At nearly all the roll attitudes there is a significant variation in force coefficient along the length of the cone, so that conical flow concepts are not likely to be helpful.

Fig 17 shows the same quantity at the first station for the three different total pressures. Separation should be laminar for all three conditions, in

accordance with the previous discussion. It is clear that Reynolds number effects are present and we can tentatively identify two of them. As the Reynolds number increases, an extra change of sign appears in the side-force variation. We can associate this with an additional feature of the nose shape becoming effective as the thickness of the boundary layer decreases. Also as the Reynolds number increases, the peak value of the side force increases. This point is pursued in Fig 18, where the numerically largest value of C_Y measured in a complete revolution in roll is plotted against Re_x, the Reynolds number based on the distance from the apex to the measuring station. Results are shown for all three unit Reynolds numbers and for all four measuring stations which lie on the conical part of the body. The increase in peak value shown in the previous Figure now appears at the left-hand side of the picture, followed by a sharp fall and a levelling off. An attempt is made to define a band within which the measurements lie. The range of values of Reynolds number over which transition might occur at the separation line is indicated. We might guess that the reduction in peak side force is associated with the turbulent reattachment phenomenon described in the previous section, since this progresses gradually in the three-dimensional flow, and obviously ends when the boundary layer is turbulent at separation.

We might hope that the consistent behaviour shown by the first five points on the left of Fig 18 would be reflected in a consistent behaviour at specific roll angles. Choosing $\phi = 270^\circ$, which is near a peak in C_Y, we obtain Fig 19, where values at all six measuring stations have been included to establish trends with more certainty. Concentrating on the left-hand edge of the plot, we see that an increase in Re_x, brought about by an increase in unit Reynolds number at station 1, produces an increase in side force, while the same increase in Re_x brought about by an increase in x produces a marked decrease in side-force coefficient.

The results at many other roll angles behave in a similar way, so we conclude that although the local Reynolds number has some value in correlating the maximum value of side-force coefficient, it does not determine the flow at particular roll angles.

In Fig 20 we present the variation of local side force coefficient with lengthwise station for four roll angles. These have been chosen, not because they are typical, but because they include the variations which are most nearly constant, and so might correspond to conical flows. In Fig 20a we might think a conical flow is emerging as the unit Reynolds number increases, but in Fig 20b the nearest approach to a constant value comes at the intermediate Reynolds

number. In Fig 20c, all the variations are small, but two distinct near-constant levels appear, a near-zero value at the two higher Reynolds numbers and a non-zero value, about the same as that in Fig 20b, at the lowest Reynolds number. In Fig 20d we see a change from a rising to a falling side force coefficient as the Reynolds number varies, with a near constant level in between.

6 CONCLUSIONS

(1) For the single line-vortex model of asymmetric conical flow over circular cones with symmetric separation lines, a thorough exploration of parameter space has revealed only insignificant regions of multiple solutions and no further bifurcation locus from which asymmetric solutions could arise.

(2) An examination of the stability of solutions of this model to small spatial disturbances has shown that stable symmetric solutions are confined to a narrow band of values of the incidence parameter, but that, with insignificant exceptions, the asymmetric solutions are stable. There is no combination of symmetric separation line position and incidence parameter for which stable symmetric and stable asymmetric solutions are both possible. The growth of disturbances to symmetric solutions is algebraic rather than exponential and the growth rates are not large.

(3) An examination of low-speed experimental data shows that asymmetric flow over a circular cone can be significantly non-conical with large variations in local side-force coefficient along the length of the cone. For a 10° cone, at an angle of incidence of 35° the approximately conical flows appear to predominate, but at 30° they occur only exceptionally.

(4) This behaviour may be described using ideas from the theory of systems of ordinary differential equations. Very near the apex, any real body departs significantly from an ideal circular cone, so the flow there defies rational description and provides initial values for the system which are essentially arbitrary. At the larger angles of incidence, for which stable conical solutions exist, the flow evolves towards a conical solution in the downstream direction, the solution acting as an attractor. This conical solution will be asymmetric at larger incidences and symmetric at smaller incidences.

LIST OF SYMBOLS

a	local radius of body cross-section
C_N	coefficient of local normal force
C_Y	coefficient of local side force
F	a particular complex function, see equation (8)
$\underline{F}(\underline{x})$	a vector function of a real vector $\underline{x}$
J	the Jacobian matrix of $\underline{F}$ with respect to $\underline{x}$
J_1	the Jacobian matrix of the stability analysis
Re_x	Reynolds number based on distance from apex, Ux/ν
U	free-stream speed
$v_1,\ldots v_4$	dependent variables in stability analysis, see equation (13)
$v_{1c},\ldots v_{4c}$	values of v_j in conical solution
$v_1',\ldots v_4'$	small variations in v_j from conical solution, equation (14)
x,y,z	right-handed rectangular Cartesian axes, see Fig 4
x_0	streamwise reference length in stability analysis
$\underline{x}$	unknown real vector
$\underline{x}_0$	approximation to solution of $\underline{F}(\underline{x}) = 0$
Z	complex variable, $y + iz$
Z_1,Z_2	complex coordinate of right-, left-hand vortex
α	angle of incidence
γ_1,γ_2	non-dimensional circulation of left-, right-hand vortex
γ_{1c},γ_{2c}	values of γ_1,γ_2 in conical solution
γ_1',γ_2'	small variations in γ_1,γ_2 from conical solution, equation (14)
Γ_1,Γ_2	circulation of right-, left-hand vortex
δ	semi-angle of circular cone
ζ_1,ζ_2	non-dimensional complex coordinates of right-, left-hand vortex
ζ_{1c},ζ_{2c}	values of ζ_1,ζ_2 in conical solution
ζ_1',ζ_2'	small variations in ζ_1,ζ_2 from conical solution
θ_1,θ_2	angular positions of right-, left-hand separation lines, see Fig 4
θ	angular position of right-hand separation line when separation is symmetric
θ_c	critical value of θ for symmetric flow
λ_r	largest real part of an eigenvalue of J_1
ν	kinematic viscosity
ξ	non-dimensional streamwise variable, see equation (6)
ϕ	angle of roll about cone axis
ψ	angular position on cone from windward generator

REFERENCES

No.	Author	Title, etc
1	A.E. Bryson	Symmetrical vortex separation on circular cylinders and cones. *J. Appl. Mech.*, (ASME), 26, 643-8 (1957)
2	D.E. Dyer S.P. Fiddes J.H.B. Smith	Asymmetric vortex separation from cones at incidence - a simple inviscid model. *Aeronautical Quart.*, 33, 293-312 (1982) Also RAE Technical Report 81330 (1981)
3	J.H.B. Smith	Improved calculations of leading-edge separation from slender, thin delta wings. *Proc. Roy. Soc. Lond.*, A, 306, 67-90 (1968) Also RAE Technical Report 66070 (1966)
4	S.P. Fiddes	A theory of the separated flow past a slender elliptic cone at incidence. Paper 30 in Computation of viscous-inviscid interaction, AGARD CP 291, 1980
5	S.P. Fiddes J.H.B. Smith	Calculations of asymmetric separated flow past circular cones at large angles of incidence. Paper 14 in Missile Aerodynamics, AGARD CP 336 (1982)
6	J.H.B. Smith	Theoretical modelling of three-dimensional vortex flows in aerodynamics. In Aerodynamics of vortical type flows in three dimensions, AGARD CP 342, 1983. Also *Aeronautical J.*, 88, 101-116 (1984)
7	S.P. Fiddes J.H.B. Smith	Asymptotic separation from slender cones at incidence. In Boundary-layer Separation, ed. F.T. Smith and S.N. Brown, Springer, 1987
8	S.P. Fiddes A.L. Williams	Recent developments in the study of separated flows past slender bodies at incidence. Paper 31 in The prediction and exploitation of separated flow. Royal Aero. Soc. Lond., 1989
9	A.L. Williams	The effect of body shape on the development of vortex asymmetry in the flow past slender bodies. Univ. of Bristol Aero Eng Rept. 413, 1990; also 17th ICAS Conf. Stockholm, 1990

REFERENCES (continued)

No.	Author	Title, etc
10	F. Marconi	Asymmetric separated flow about sharp cones in a supersonic stream. Proc. 11th Int. Conf. Num. Meth. in Fluid Dyn., Lecture Notes in Physics 323, Springer, 1989
11	M.J.Siclari F. Marconi	The computation of Navier-Stokes solutions exhibiting asymmetric vortices. AIAA Paper 89-1817, 1989
12	B.L. Hunt	Asymmetric vortex forces and wakes on slender bodies. AIAA Paper 82-1336, 1982
13	S.P. Fiddes D.E. Lean I.R.M. Moir	Experimental investigation of the separated flow past slender bodies in the RAE 5 metre low-speed pressurised tunnel. RAE Technical Memorandum Aero 2209 (1991)
14	S.P. Fiddes	Separated flow about cones at incidence - theory and experiment. In Studies of vortex dominated flows, Ed. M.Y. Hussaini and M.D. Salas, Springer, 1987
15	T.B. Benjamin	Bifurcation phenomena in steady flows of a viscous fluid. *Proc. Roy. Soc. Lond. A.*, 359, 1-26, 1978
16	S. Chin C.E. Lan	Calculation of symmetric and asymmetric vortex separation on cones and tangent ogives based on discrete vortex models. NASA CR 4122, 1988
17	W.J. Rainbird R.S. Crabbe D.J. Peake R.F. Meyer	Some examples of separation in three-dimensional flows. *CASI J.*, 12, 10, 409-423 (1966)
18	A.R.G. Mundell	RAE unpublished
19	Katherine Moore	Line-vortex models of separated flow past a circular cone at incidence. RAE Technical Memorandum Aero 1917 (1981)
20	D.W. Jordan P. Smith	Nonlinear ordinary differential equations. Clarendon Press, Oxford, 2nd Ed., 1987

REFERENCES (concluded)

No.	Author	Title, etc
21	I.R.M. Moir	Recent experiences in the RAE 5 metre Wind Tunnel of a china clay method for indicating boundary layer transition. *Aeronautical J.*, 90, 6-9, 1986

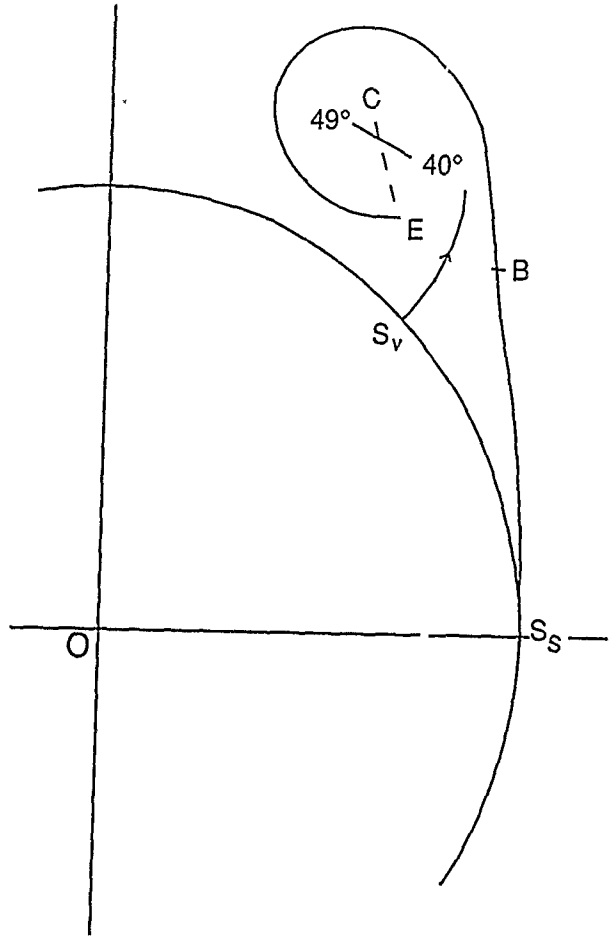

Fig 1 Comparison of line-vortex and sheet-vortex models for symmetrical flow past a circular cone

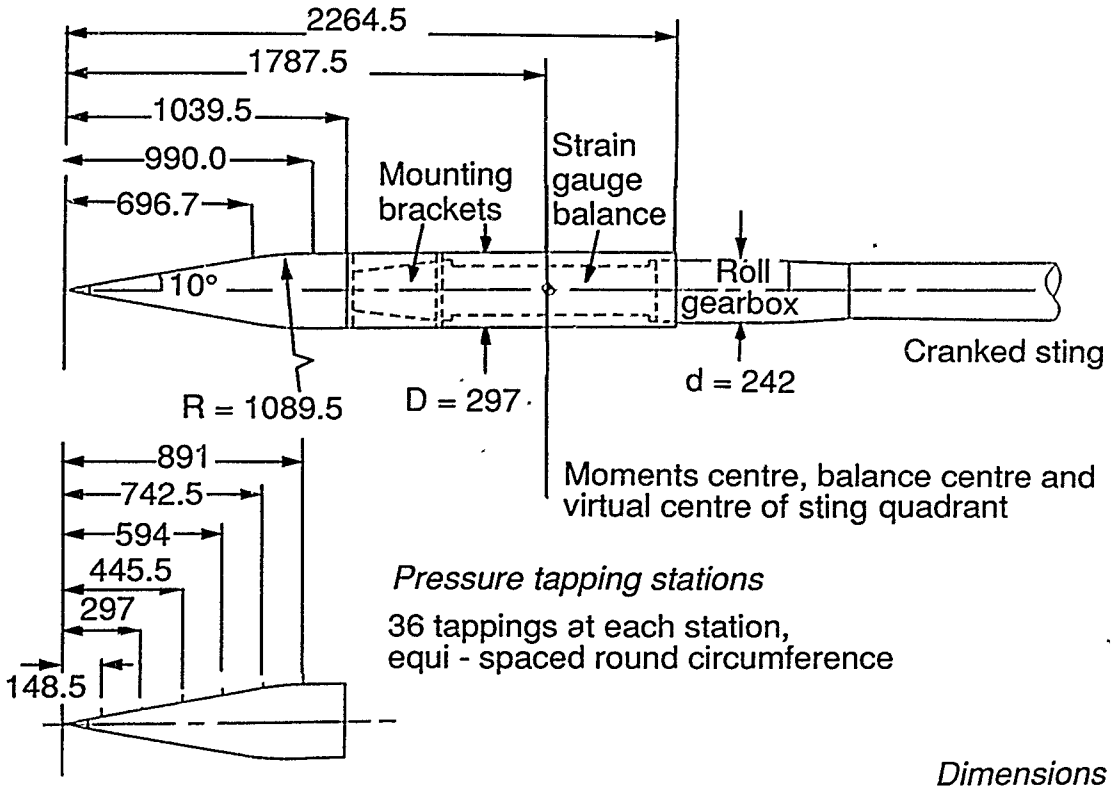

Fig 2 Details of cone-cylinder model

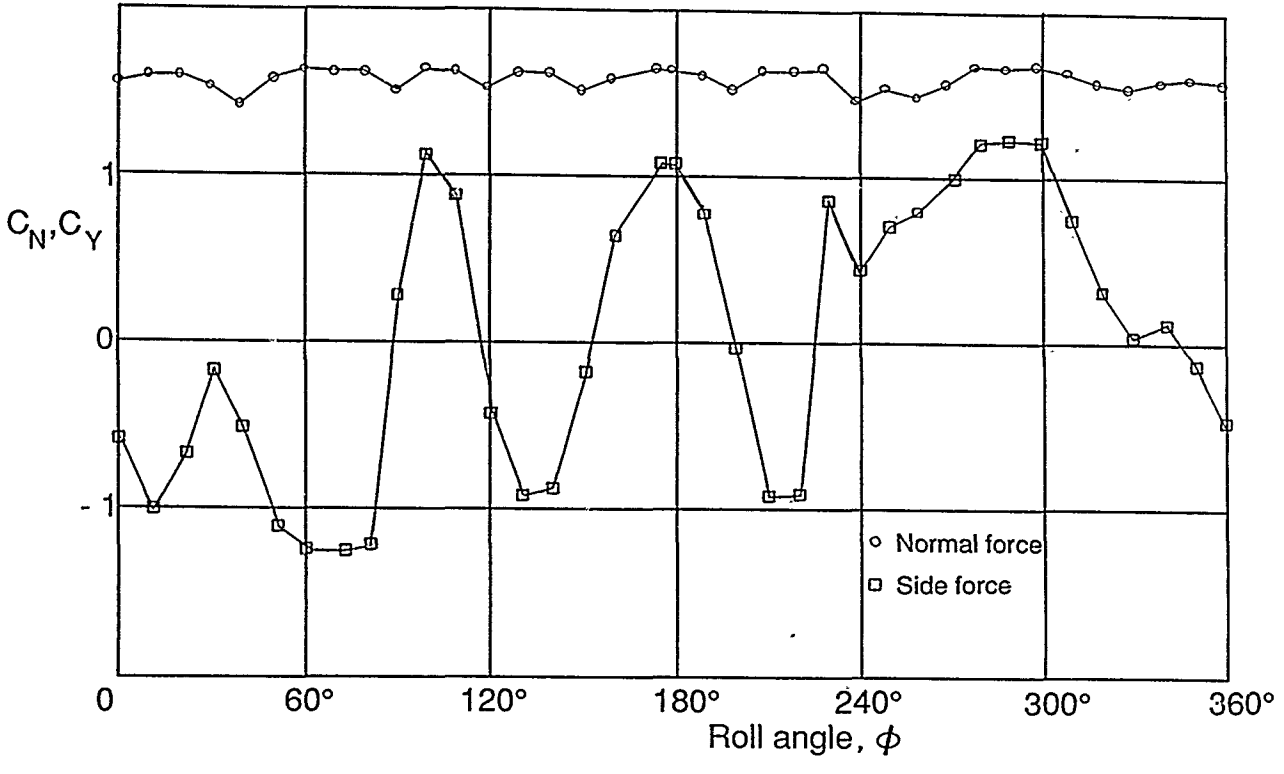

Fig 3 Variation of local side and normal force with roll angle at station 1, $\alpha = 35°$

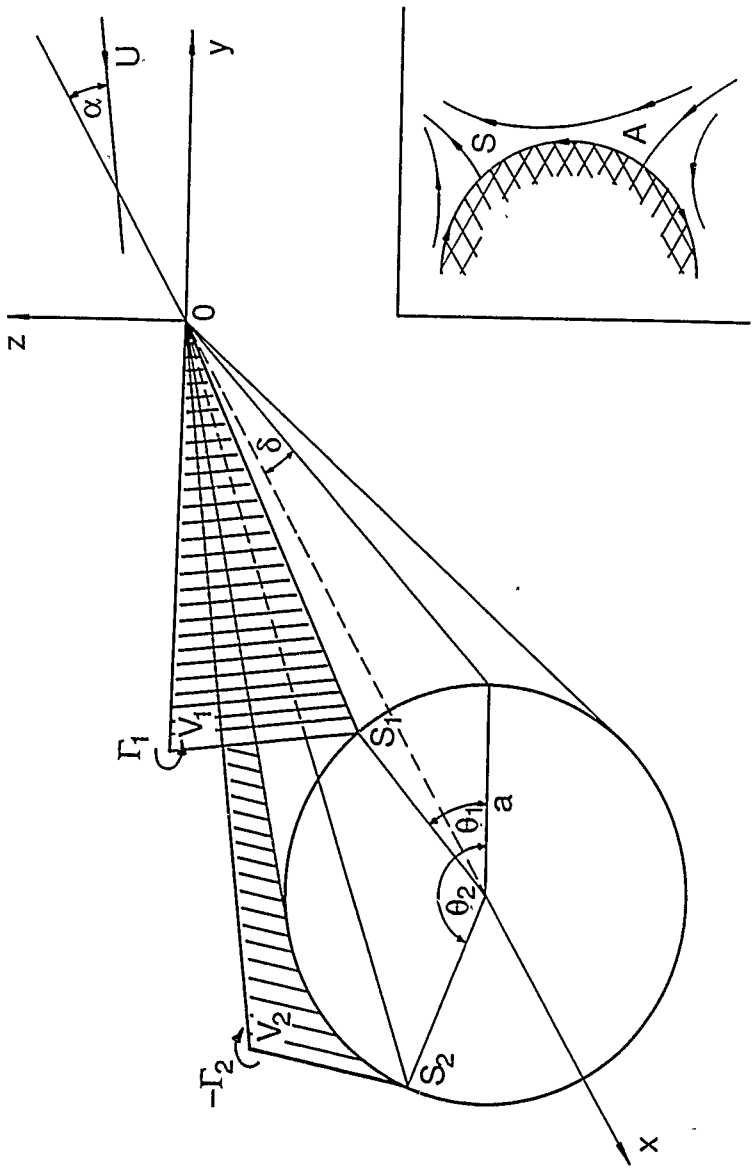

Fig 4 Configuration and coordinate system (inset: flow structure)

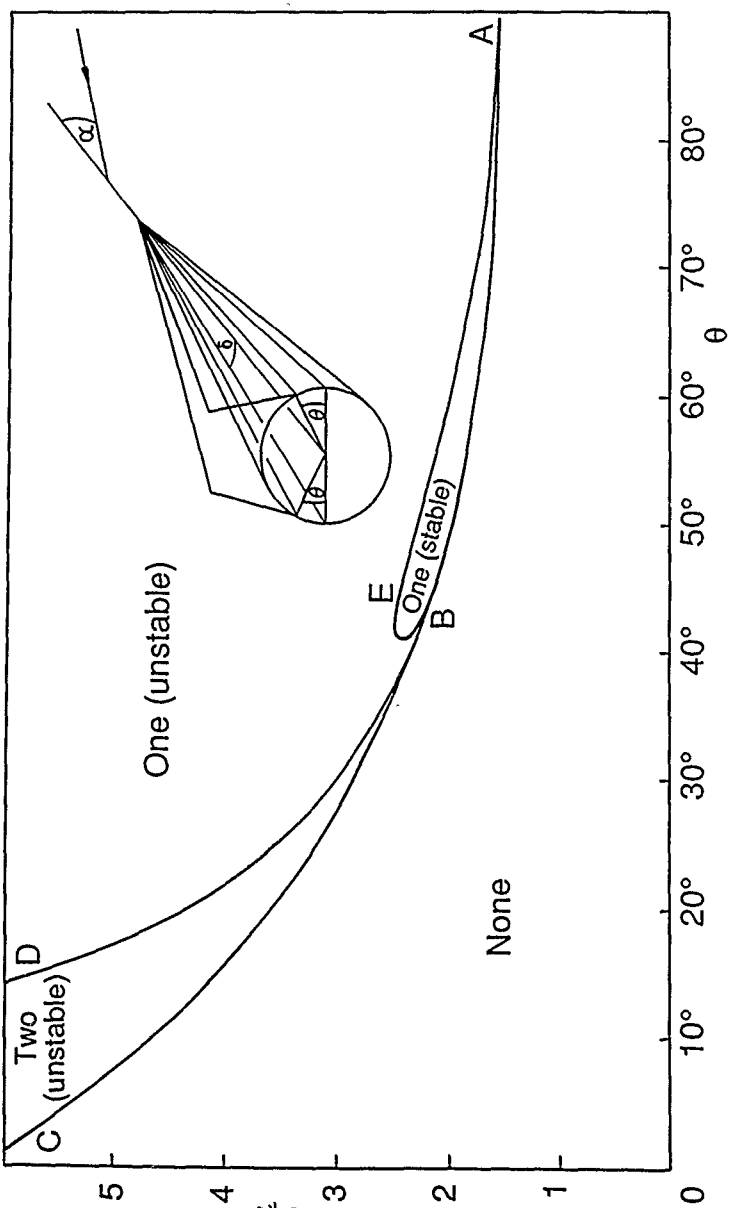

Fig 5 Range of symmetric solutions

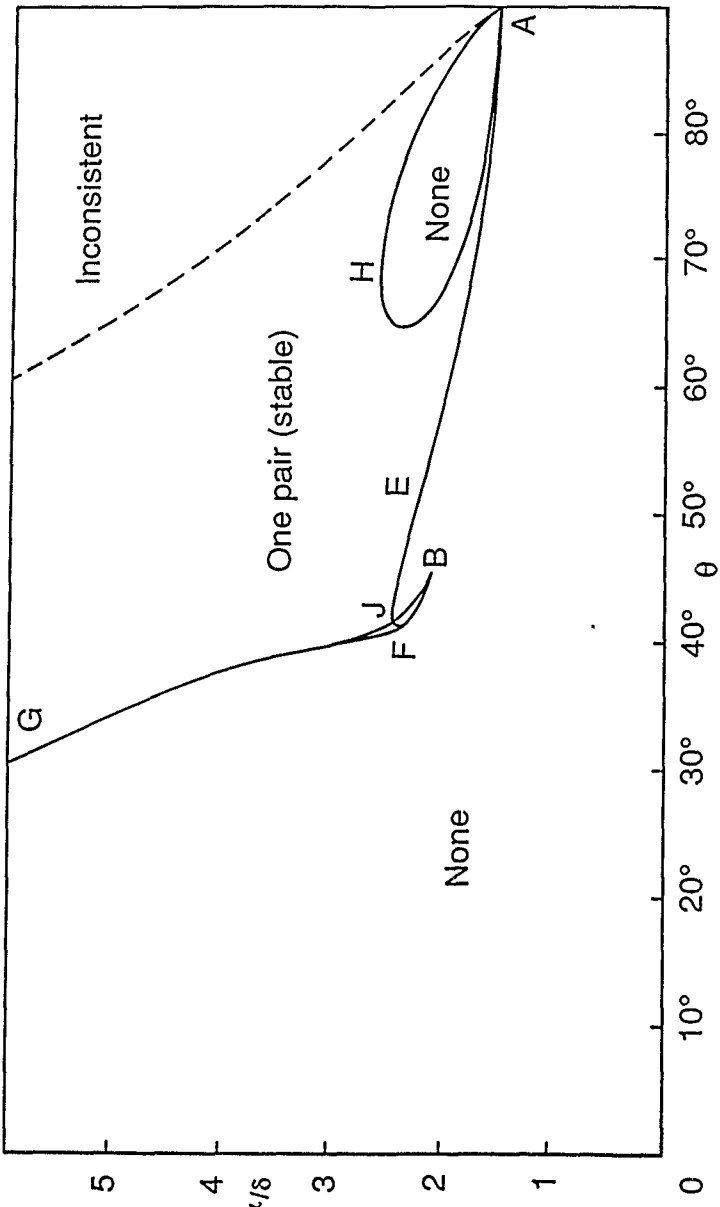

Fig 6 Range of asymmetric solutions

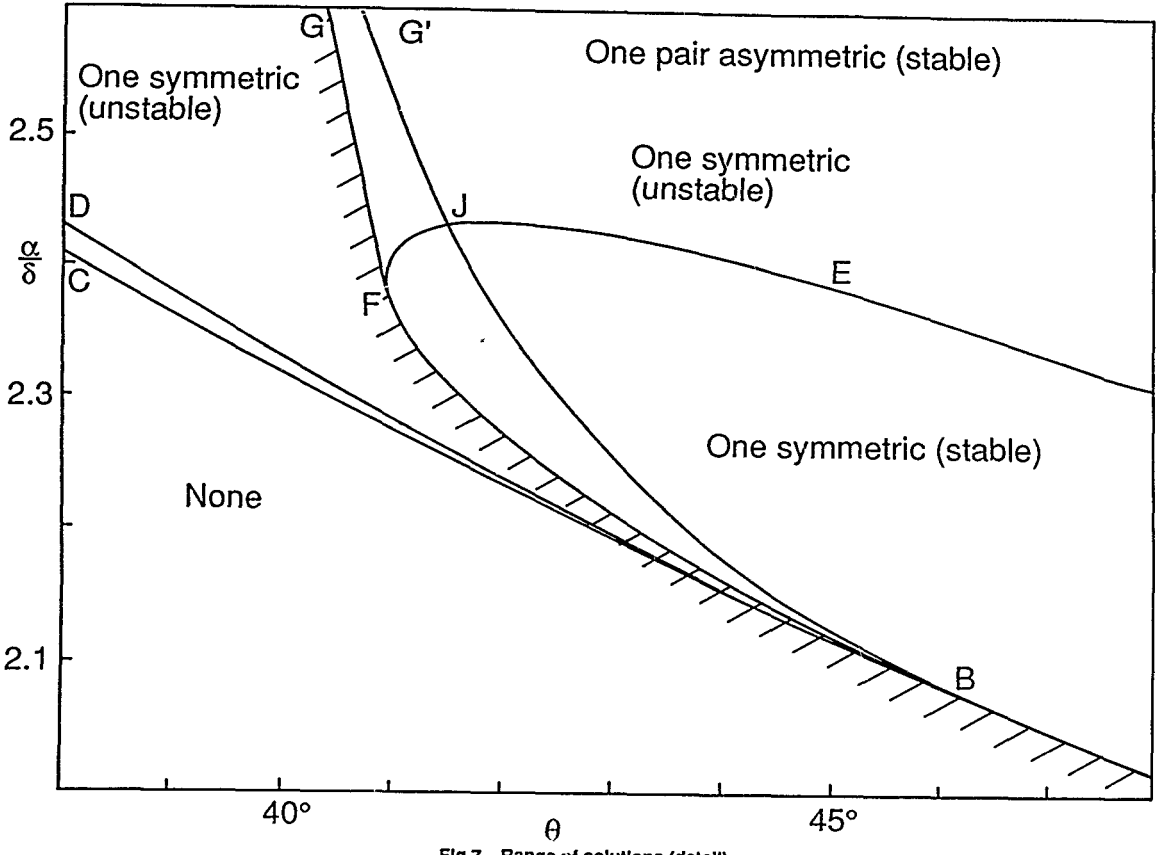

Fig 7 Range of solutions (detail)

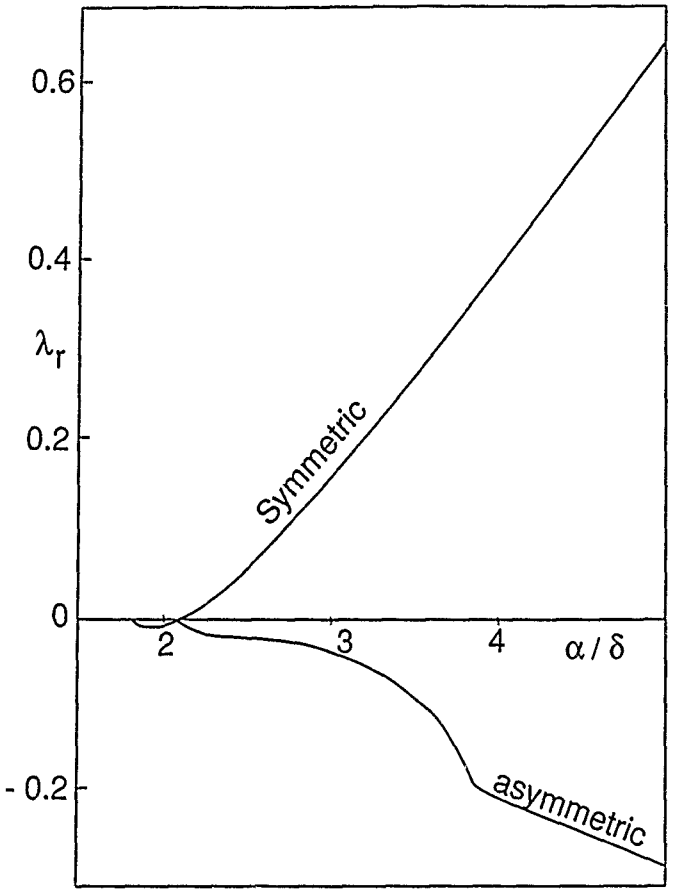

Fig 8 Real part of dominant eigenvalue, $\theta = 56.0°$

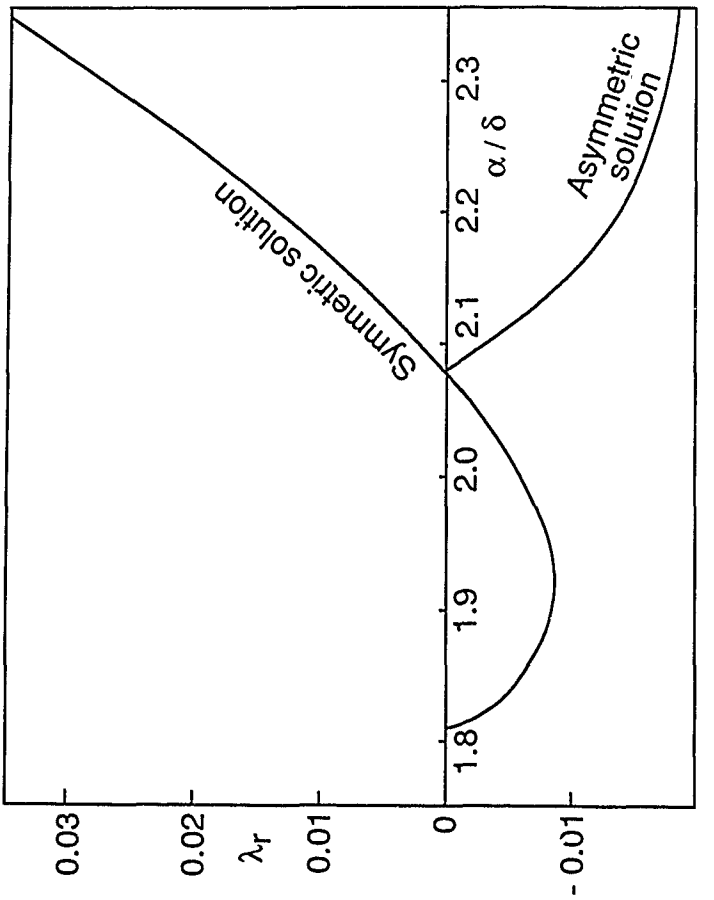

Fig 9 Real part of dominant eigenvalue for $\theta_s = 56°$

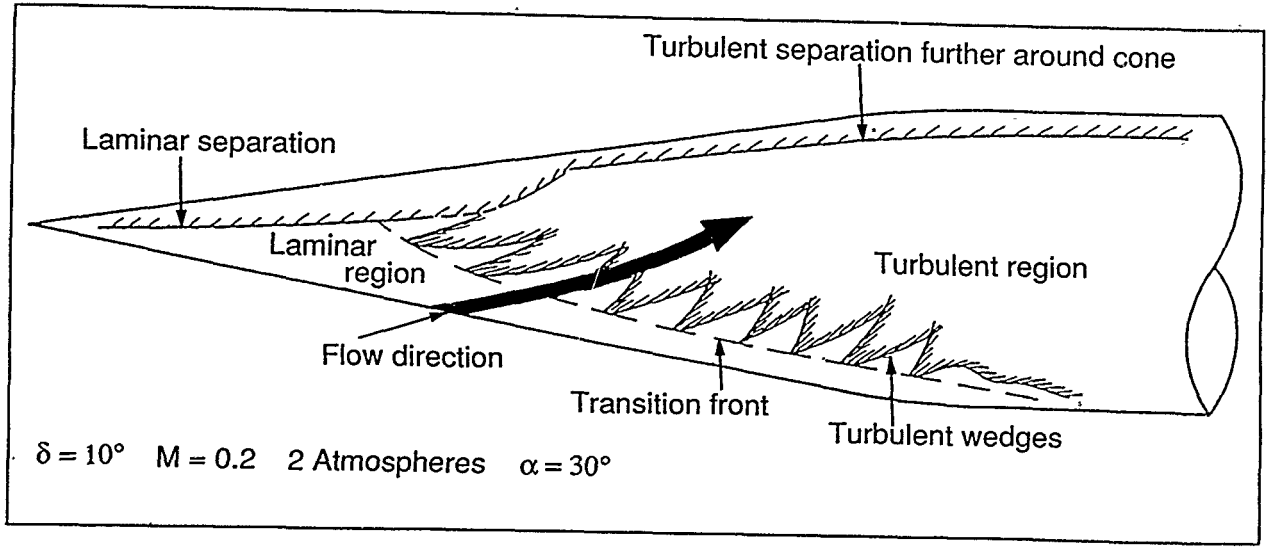

Fig 10 Transition and separation on tunnel model

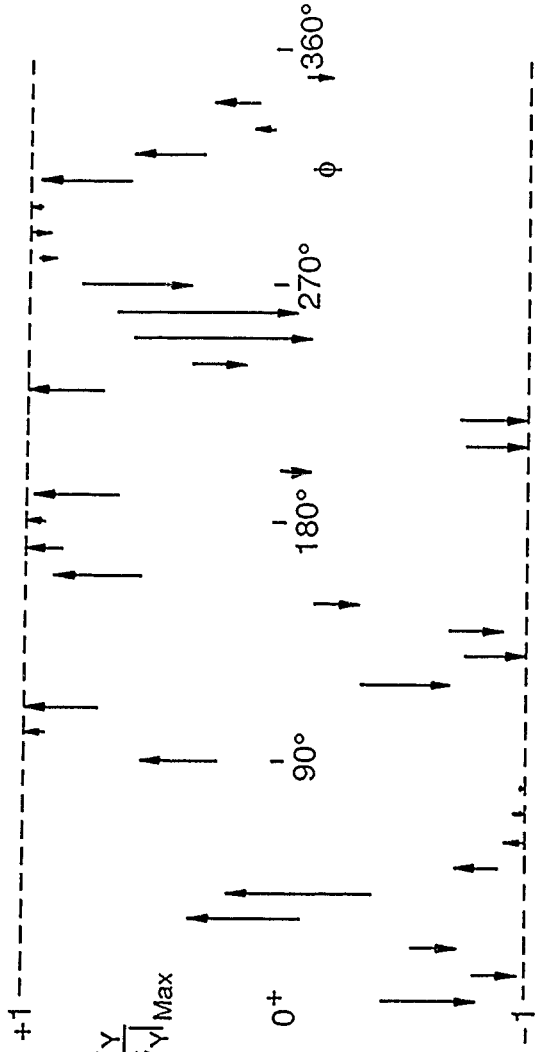

Fig 11 Shift in side-force between stations 1 and 2, $\alpha = 35°$, $Re_D = 1.0 \times 10^6$

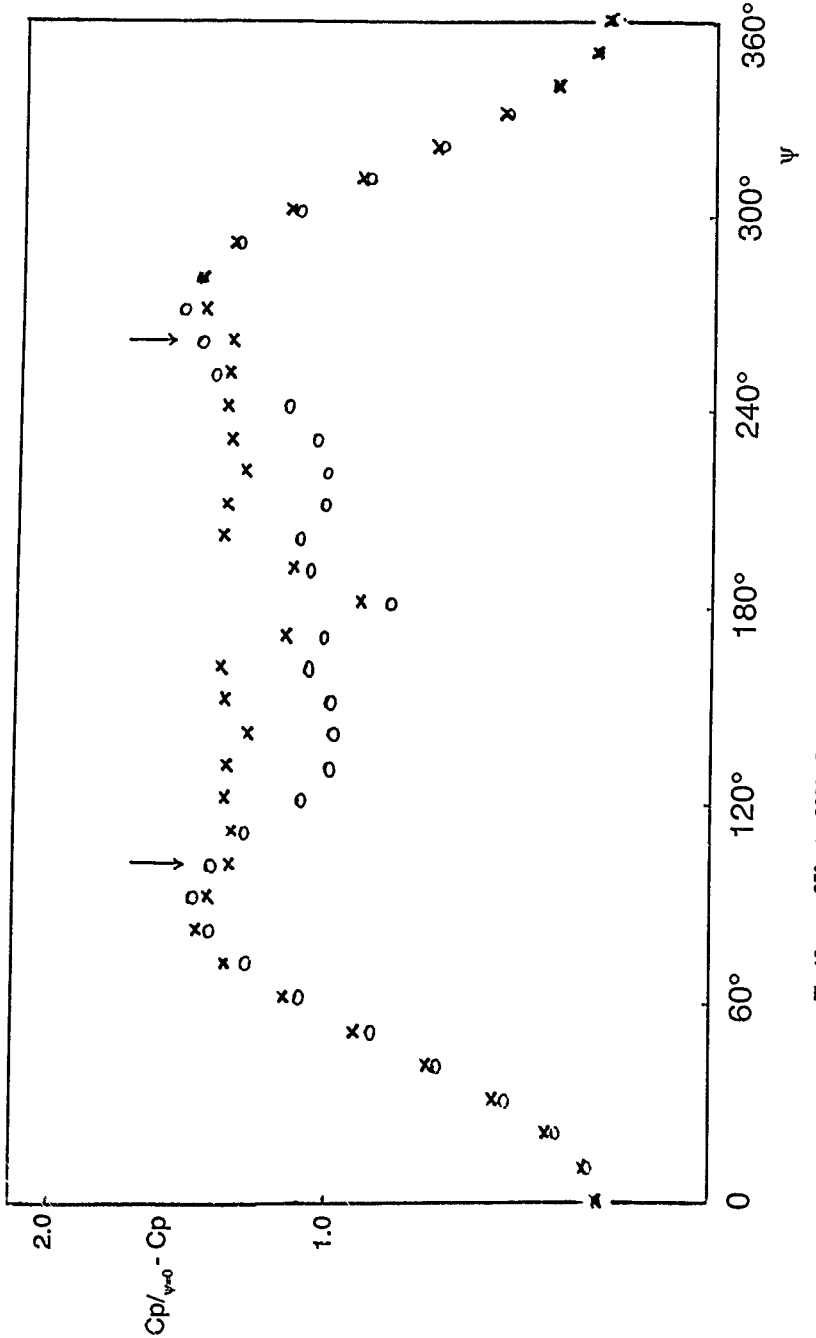

Fig 12 $\alpha = 35°$, $\phi = 330°$, Cp adjusted to agree at $\psi = 0$: stations 1(x) and 2(0)

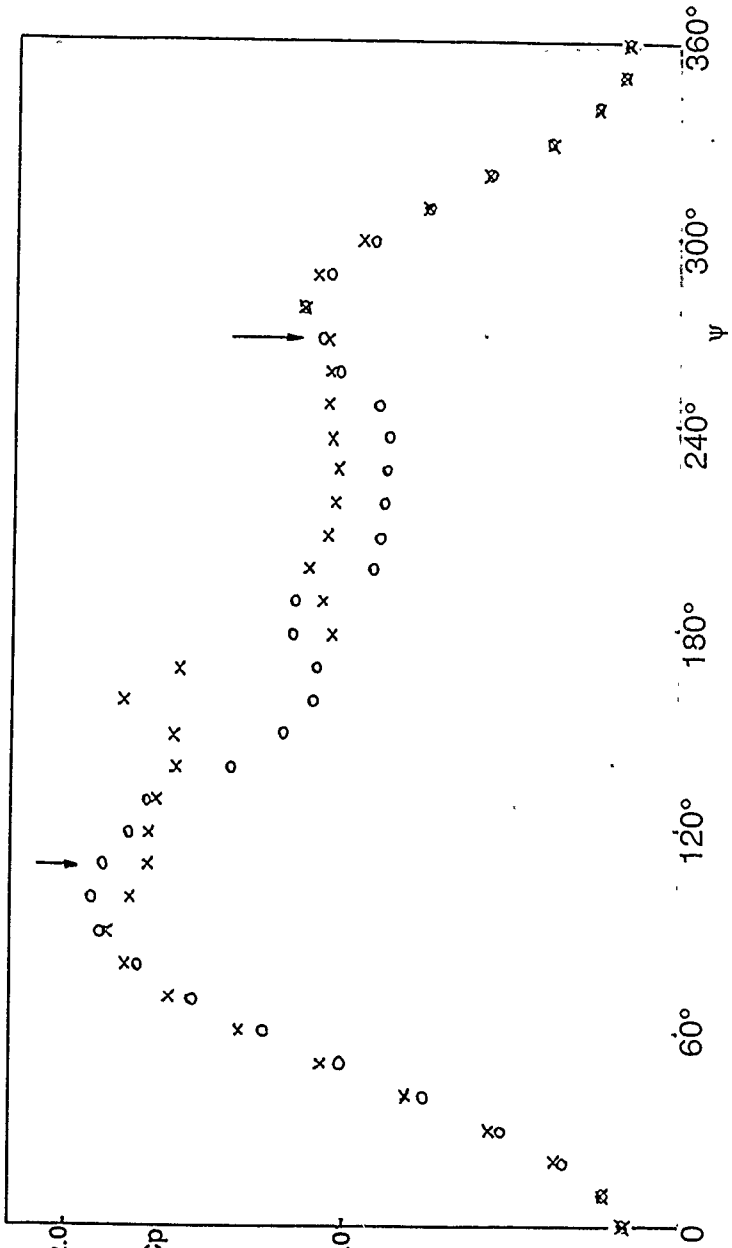

Fig 13 $\alpha = 35°$, $\phi = 180°$, C_p adjusted to agree at $\psi = 0$: stations 1(x) and 2(0)

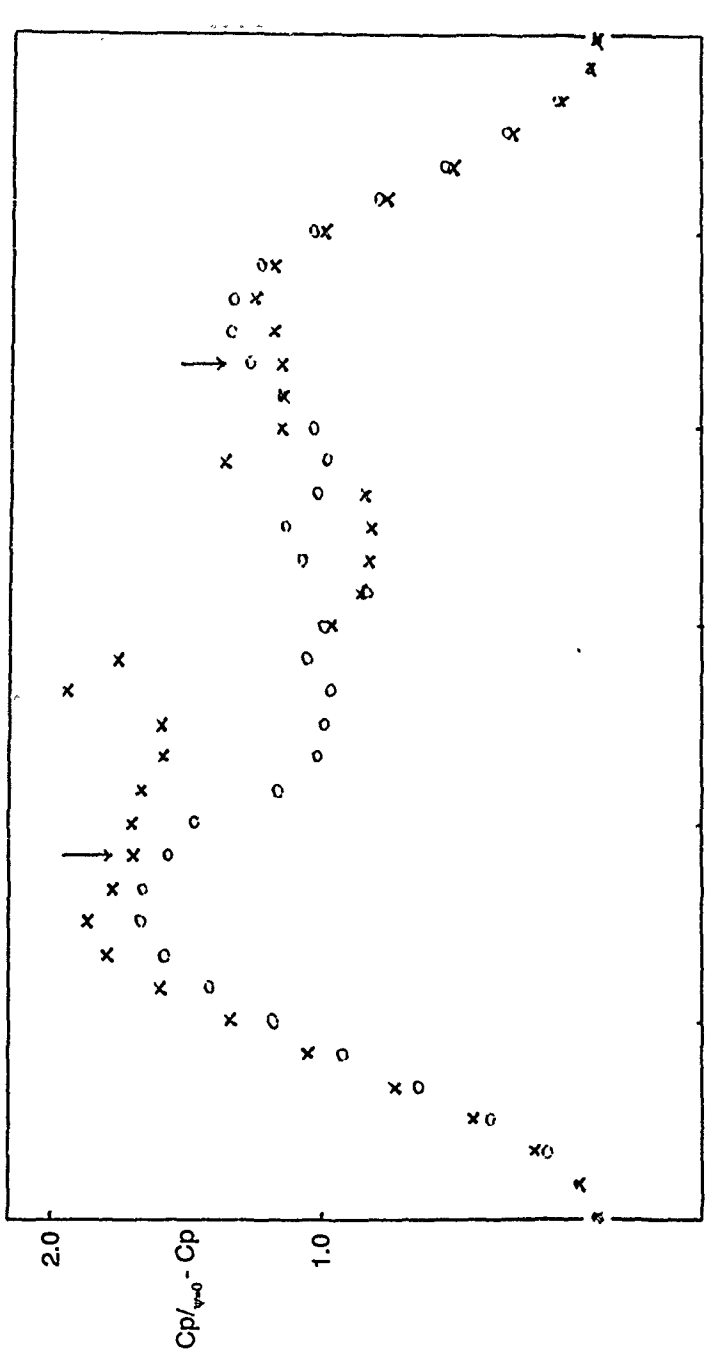

Fig 14 $\alpha=35°$, $\phi=270°$, C_p adjusted to agree at $\psi=0$: stations 1(x) and 2(0)

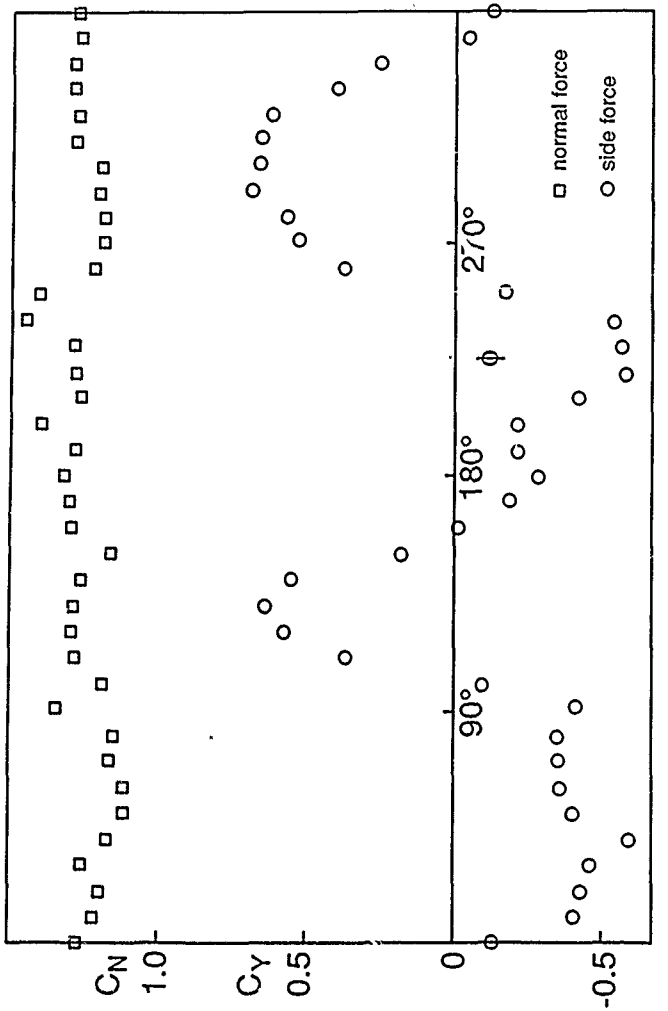

Fig 15 Local force coefficient vs roll angle
$\alpha = 30°$, station 1, $P_t = 110$ kPa

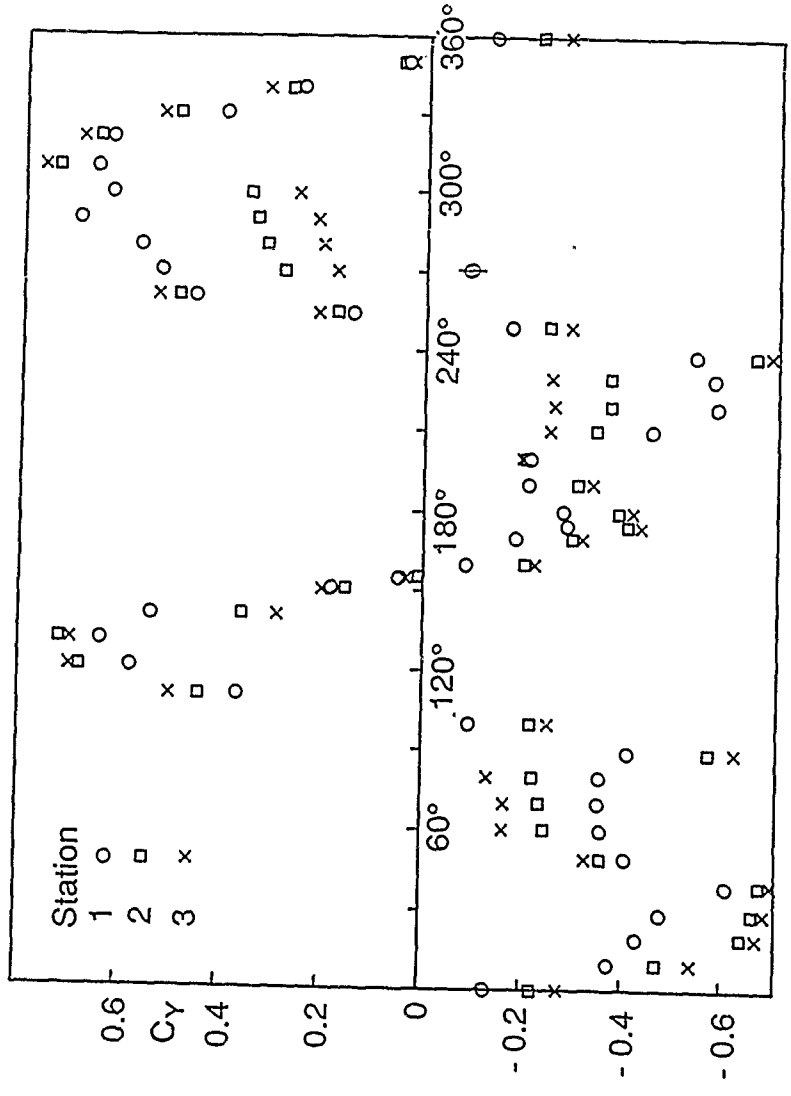

Fig 16 Local side-force coefficient vs roll angle
$\alpha = 30°$, $P_t = 110$ kPa

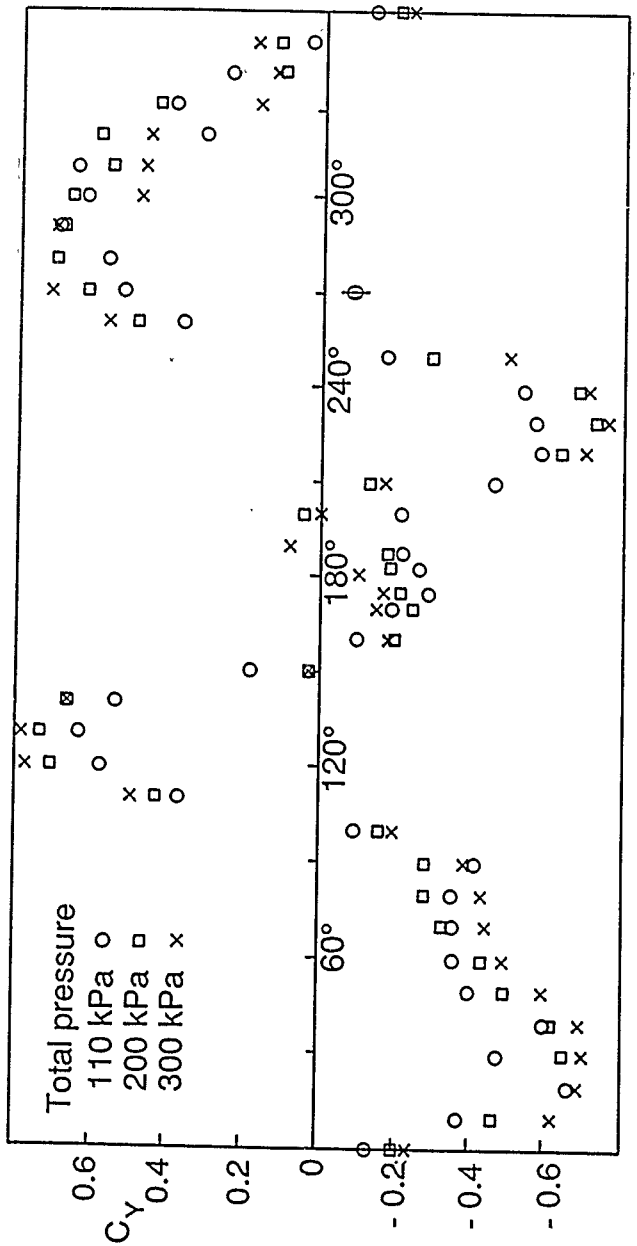

Fig 17 Local side-force coefficient vs roll angle
$\alpha = 30°$, station 1

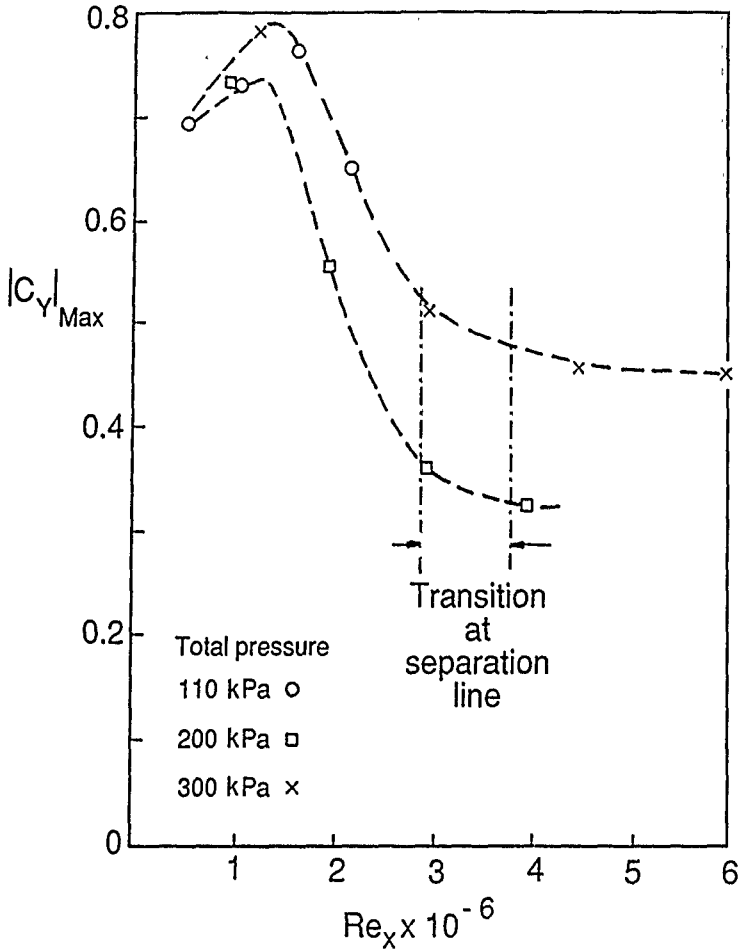

Fig 18 Peak side-force coefficient vs local Reynolds number
$\alpha = 30°$

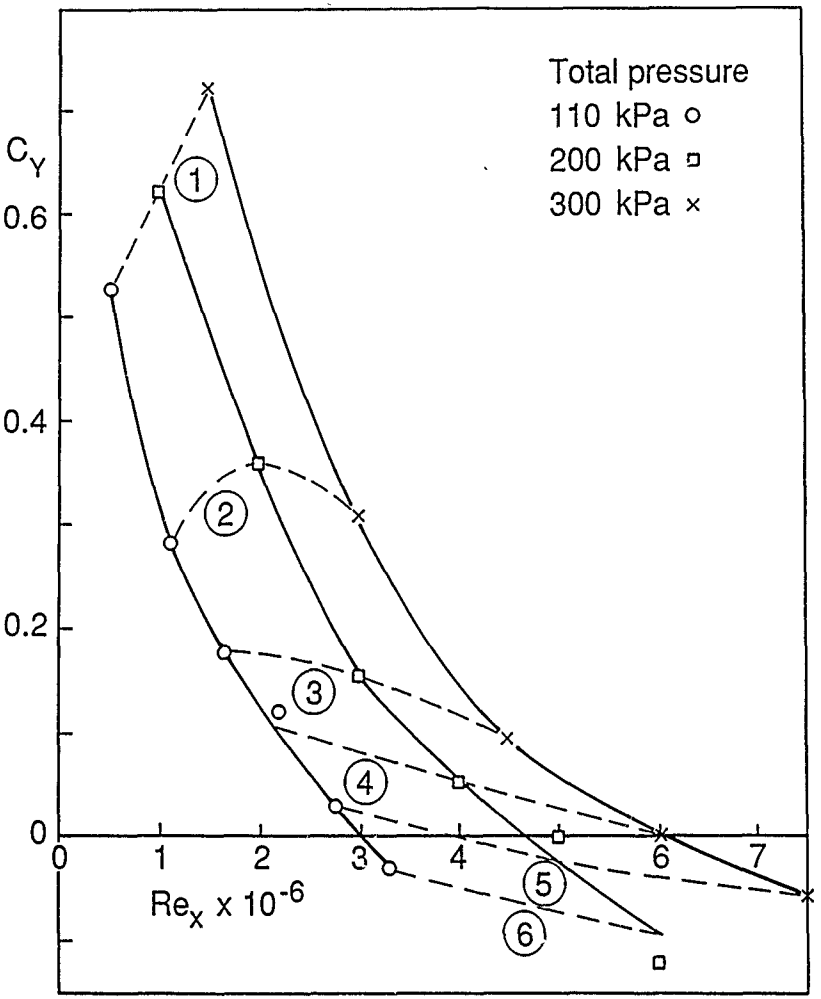

Fig 19 Side-force coefficient vs local Reynolds number
$\alpha = 30°$, $\phi = 270°$

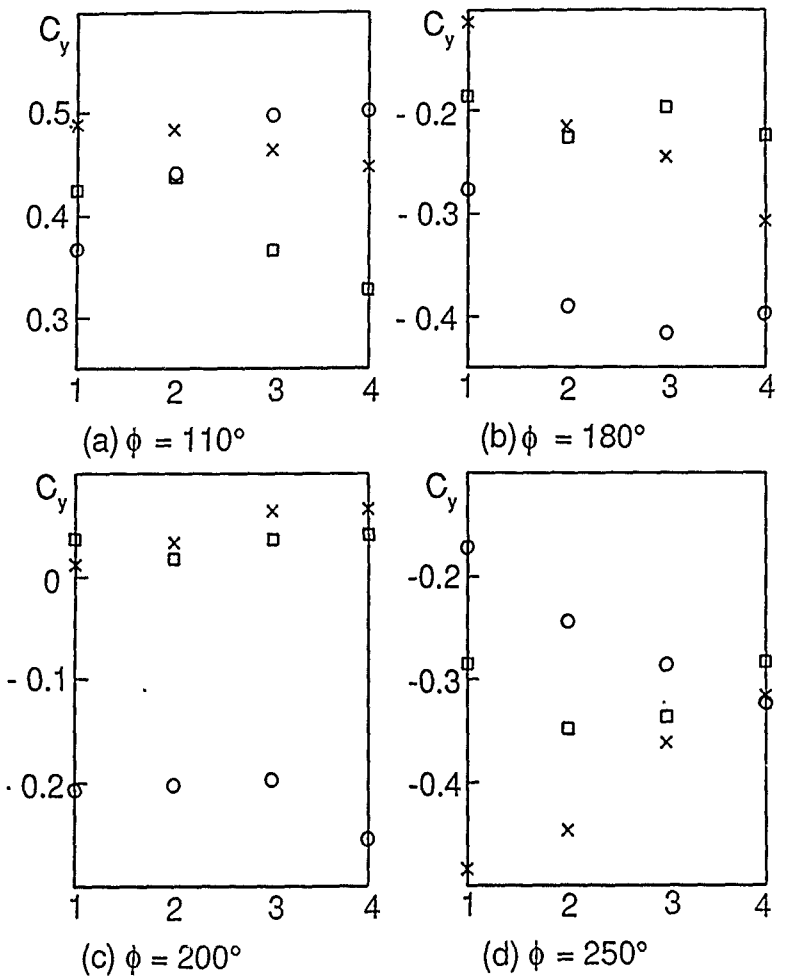

Fig 20 Variation of local side-force coefficient along cone for total pressure 110(0), 200(□) and 300 (X) kPa

REPORT DOCUMENTATION PAGE

Overall security classification of this page

UNLIMITED

As far as possible this page should contain only unclassified information. If it is necessary to enter classified information, the box above must be marked to indicate the classification, e.g. Restricted, Confidential or Secret.

1. DRIC Reference (to be added by DRIC)	2. Originator's Reference	3. Agency Reference	4. Report Security Classification/Marking
	RAE TM Aero 2211		UNLIMITED

5. DRIC Code for Originator	6. Originator (Corporate Author) Name and Location
7673000W	Royal Aerospace Establishment, Farnborough, Hants, UK
5a. Sponsoring Agency's Code	6a. Sponsoring Agency (Contract Authority) Name and Location

7. Title Asymmetric vortex flow over circular cones

7a. (For Translations) Title in Foreign Language

7b. (For Conference Papers) Title, Place and Date of Conference

8. Author 1, Surname, Initials	9a. Author 2	9b. Authors 3, 4	10. Date	Pages	Refs.
Pidd, M.	Smith, J.H.B.		March 1991	45	21

11. Contract Number	12. Period	13. Project	14. Other Reference Nos.
		N/A	

15. Distribution statement

(a) Controlled by –

(b) Special limitations (if any) –

If it is intended that a copy of this document shall be released overseas refer to RAE Leaflet No.3 to Supplement 6 of MOD Manual 4.

16. Descriptors (Keywords) (Descriptors marked * are selected from TEST)

Vortices*. Boundary-layer separation*. Slender-body theory.

17. Abstract

Asymmetric vortex flow over circular cones is discussed in the light of predictions of the single-line-vortex model and of measurements made by Fiddes, Moir and Lean in the RAE 5m Wind Tunnel. For the case of separation lines specified as laterally symmetric, the space of conical solutions which contains the symmetric solutions of Bryson is explored thoroughly. No more than one pair of asymmetric solutions is found for each combination of a separation position and a ratio of incidence to cone semi-angle, except in a small region of the parameter space. The stability of the solutions to small asymmetric spatial disturbances is calculated. It emerges there is nowhere more than one stable solution, symmetric at smaller incidences, asymmetric at larger.

In contrast, the experiment, on a 10° semi-angle cone, with laminar separation, reveals many different levels of local side force, depending on roll angle, lengthwise station, and unit Reynolds number, as well as incidence. It is shown that the flow can be highly non-conical. At 35° incidence the flow may be developing streamwise towards a conical state, but this is not apparent at 30°.

F5910/1

RAE Form A143 (revised October 1980)

No room for full stop